Controlled Hydrothermal Crystallization of Anhydrous $Ln_2(OH)_4SO_4$ as A New Family of Layered Rare-Earth Hydroxide (Ln=Eu-Lu and Y)

Xuejiao Wang,[a,b,c,d*] Maxim S. Molokeev,[e,f,g] Qi Zhu,[c,d] and Ji-Guang Li[b,c,d*]

[a]College of New Energy, Bohai University, Jinzhou 121000, China

[b]Research Center for Functional Materials, National Institute for Materials Science, Tsukuba, Ibaraki 305-0044, Japan

[c]Key Laboratory for Anisotropy and Texture of Materials (Ministry of Education), Northeastern University, Shenyang, Liaoning 110819, China

[d]Institute of Ceramics and Powder Metallurgy, School of Materials Science and Engineering, Northeastern University, Shenyang, Liaoning 110819, China

[e]Laboratory of Crystal Physics, Kirensky Institute of Physics, Federal Research Center KSC SB RAS, Krasnoyarsk 660036, Russia

[f]Department of Physics, Far Eastern State Transport University, Khabarovsk 680021, Russia

[g]Siberian Federal University, Krasnoyarsk 660041, Russia

*Corresponding author

Dr. Xuejiao Wang

Bohai University, China

Tel: +86-416-3400708

E-mail: wangxuejiao@bhu.edu.cn

Dr. Ji-Guang Li

National Institute for Materials Science, Japan

Tel: +81-29-860-4394

E-mail: li.jiguang@nims.go.jp

ABSTRACT

The anhydrous hydroxyl sulfate of $Ln_2(OH)_4SO_4$ (Ln=Eu-Lu and Y) has been successfully synthesized in this work as a new family of layered rare-earth hydroxide (LRH) via controlled hydrothermal crystallization. Crystal structure decipherment revealed that the compounds crystallize in the monoclinic system (space group: *C*2/*m*), with the structure built up *via* alternative stacking of the interlayer SO_4^{2-} and the two-dimensional host layer, composed of three-capped [LnO_9] trigonal prisms, along the *a*-axis. Distinctly different from the recently reported hydrated LRH of $Ln_2(OH)_4SO_4{\cdot}2H_2O$ (only existing for Ln=La-Dy), the host layers of the anhydrous phase are linked together *via* sharing edges instead of O node of the SO_4^{2-} tetrahedron. Rietveld refinement found that the lattice parameters and cell volume tend to decrease towards a smaller Ln^{3+} while the axis angle (β=98.78-100.31°) behaves oppositely. Comparative TG/DTA analysis of the $Ln_2(OH)_4SO_4$ in air revealed that the occurrence temperature range of $Ln_2O_2SO_4$ narrows towards a smaller Ln^{3+} owing to the gradually higher and lower temperatures of dehydroxylation (up to ~500 °C) and desulfurization, respectively. The newly discovered $Ln_2(OH)_4SO_4$, together with the aforementioned hydrated LRH family, allows for the first time the green synthesis of $Ln_2O_2SO_4$ with water as the only exhaust for the full spectrum of lanthanides (Ln=La-Lu and Y). Calcining $Ln_2(OH)_4SO_4$ in H_2 yielded phase pure Ln_2O_2S for Eu and Gd while a mixture of Ln_2O_2S and Ln_2O_3 for the rest of Ln. The effects of lanthanide contraction on the crystallization behavior, thermolysis, and phase evolution upon calcination of the anhydrous LRH compounds as well as the structural parameters of the products were clearly revealed. The photoluminescence was also detailed for the anhydrous LRH of Eu and Tb.

Keywords: anhydrous hydroxyl sulfate; crystal structure; oxysulfate; oxysulfide; photoluminescence

■ INTRODUCTION

Layered inorganic compounds have been finding wide applications in the fields of drug delivery,[1] catalysis,[2] high performance microelectronics,[3] flame retardants,[4] hydrogel,[5] UV shielding,[6] and luminescence.[7] Layered rare-earth hydroxide (LRH) beneficially combines a layered crystal structure and the abundant and unique optical, magnetic and catalytic functionalities of the rare-earth elements, and is thus of great research interest.[8-11] The group of layered compounds has the general formula of $Ln_2(OH)_{6-m}(A^{x-})_{m/x}\cdot nH_2O$, where Ln is a trivalent rare-earth ion, A is a guest anion, $1.0 \leq m \leq 2.0$, and n=0-2. The study on LRH can be dated back to the late 1960s and is exemplified by the work on $Ln(OH)_2A$ ($A=Cl^-$ or NO_3^-), which consists of alternating hydrogen-bonded $[Ln(OH)_2]^+$ and A^- layers.[12,13] LRH gained new attention since Gándara *et al.* reported in 2006 that the layered metal-organic framework (MOF) of $[Ln_4(OH)_{10}(H_2O)_4]_nA_n$ (Ln=Ho, Dy, Yb and Y; $A=NDS^{2-}$ and $AQDS^{2-}$) can be a superior heterogeneous catalyst because of its ability to facilely vary the coordination number in the catalysis process.[8] The subsequent efforts on synthesis,[14,15] interlayer exploration[16,17] and structure characterization[18-20] have identified that the $Ln_2(OH)_5A\cdot 1.5H_2O$ family (A=halogen or NO_3^- anion; m=1, x=1, and n~1.5 in the general formula) is generally capable of facile anion exchange and intercalation, and since then exfoliation of $Ln_2(OH)_5A\cdot 1.5H_2O$ crystals into nanosheets[21,22] and further functionalization with either the pristine crystallites or exfoliated nanosheets have been achieved.[23-25] It is generally observed that this group of LRH is more readily crystallized for the intermediately sized Ln^{3+} (Ln=Sm-Tm and Y) by the well-established synthetic strategies of refluxing (homogeneous precipitation),[18,26]

hydrothermal reaction,[27] and controlled titration.[15] The LRHs of the larger sized La^{3+} and Nd^{3+} were obtained by Byeon *et al. via* solvothermal reaction of the corresponding nitrate and AOH (A=K, Rb, or Cs) in ethanol, and their ability to undergo anion exchange and exfoliation was also demonstrated.[28] For the second smallest lanthanide ion of Yb^{3+}, Fogg *et al.* found that the product tends to be a mixture of the three layered phases of $Yb_2(OH)_5NO_3{\cdot}nH_2O$, where n=1.0, 1.5 and 2.0, respectively, and the anion exchangeable $Yb_2(OH)_5NO_3{\cdot}1.5H_2O$ was isolated by applying kinetic control.[10] For the smallest Lu^{3+}, phase pure LRH has not been reported to the best of our knowledge.

The sulfate-type LRH of $Ln_2(OH)_4SO_4{\cdot}2H_2O$ ($A=SO_4^{2-}$; m=2, x=2, and n~2 in the general formula) was synthesized by Sasaki's group in 2010 *via* refluxing a mixed solution of $Ln_2(SO_4)_3{\cdot}8H_2O$, Na_2SO_4 and hexamethylenetetramine (homogenous precipitation),[29] and its crystal structure was subsequently studied in detail.[30,31] It was found that this new category of LRH distinguishes itself from the $Ln_2(OH)_5A{\cdot}1.5H_2O$ family in that its hydroxide host layers exclusively consist of LnO_9 polyhedra, with the interlayer SO_4^{2-} bidentatedly coordinated to the Ln center (un-exchangeable), while those of $Ln_2(OH)_5A{\cdot}1.5H_2O$ are constructed *via* edge sharing of LnO_8 ($[Ln(OH)_7H_2O]$) and LnO_9 ($[Ln(OH)_8H_2O]$) polyhedra, with the interlayer anions existing as free ones for charge compensation.[15,27,32,33] From the view point of chemical composition, one unique feature of $Ln_2(OH)_4SO_4{\cdot}2H_2O$ is that it has exactly the same Ln/S molar ratio of the rare-earth oxysulfate ($Ln_2O_2SO_4$) and oxysulfide (Ln_2O_2S), two important groups of compounds that have diverse functionalities. Ln_2O_2S, for example, is well-known as a host lattice for efficient luminescence and is being widely used in the fields of ultraviolet light emitting diodes (UV-LEDs),

persistent luminescence, cathode-ray tubes (CRTs), plasma display panels (PDPs), and X-ray computed tomography (X-CT).[34-37] $Ln_2O_2SO_4$ can act as the precursor to fabricate Ln_2O_2S and itself also finds promising applications in oxygen storage, catalysis, and luminescence.[38-41] The traditional synthesis of $Ln_2O_2SO_4$ and Ln_2O_2S is generally independent of the harmful reactant/exhaust of elemental sulfur, $Na_2S_2O_3$, H_2S, CS_2, SO_x and so forth. In this regard, $Ln_2(OH)_4SO_4{\cdot}2H_2O$ is an ideal precursor since its unique Ln/S molar ratio allows simple dehydration and dehydroxylation of this type of LRH under proper annealing to yield $Ln_2O_2SO_4$ and Ln_2O_2S with water as the only by-product.[29,42]

The sulfate-type LRH seems limited to the larger lanthanide ions of Pr-Tb by the aforementioned homogeneous precipitation technique.[29] We recently performed $Ln_2(OH)_4SO_4{\cdot}2H_2O$ synthesis *via* hydrothermal reaction of Ln nitrate and ammonium sulfate, and successfully extended the family to Ln=La-Dy (excluding Ce and Pm).[42] In our further efforts to expand the sulfate family of LRH compounds, we identified the anhydrous hydroxyl sulfate of $Ln_2(OH)_4SO_4$ as a new type of LRH for the relatively smaller lanthanide ions of Eu-Lu (including Y). This newly discovered group of LRH, together with the hydrated $Ln_2(OH)_4SO_4{\cdot}2H_2O$ reported recently, allows the green synthesis of $Ln_2O_2SO_4$ for the whole lanthanide series (including Y) and also provides an opportunity to explore the effects of lanthanide contraction on the structural feature and stability of $Ln_2O_2SO_4$ and Ln_2O_2S. In the following sections, we report the selective crystallization, crystal structure, and thermolysis of $Ln_2(OH)_4SO_4$ as well as the phase transition upon calcination. The photoluminescence properties were also detailed for the anhydrous LRH of Eu and Tb.

■ MATERIALS AND METHODS

Reagents and Synthesis. $Ln(NO_3)_3 \cdot 6H_2O$ (Ln=La-Lu and Y, 99.99% pure), $(NH_4)_2SO_4$ (>99.5% pure), and $NH_3 \cdot H_2O$ solution (ultrahigh purity) were purchased from Kanto Chemical Co. Inc. (Tokyo, Japan) and were used as received. Milli-Q filtered water (resistivity >18 MΩ·cm) was used throughout the experiments. $Ln(NO_3)_3 \cdot 6H_2O$ was dissolved in water to make Ln^{3+} solution of 0.1 mol/L. In a typical synthesis, 6 mmol $(NH_4)_2SO_4$ particles (0.79284 g) were dissolved in 60 mL of the Ln^{3+} solution (6 mmol of Ln^{3+}), followed by dropwise addition of $NH_3 \cdot H_2O$ for pH adjustment. The resultant turbid solution was homogenized at room temperature under magnetic stirring for 10 min before being transferred to a Teflon lined stainless steel autoclave of 100 mL capacity for 24 h of hydrothermal crystallization in an air oven preheated to a predetermined temperature. The resultant solid was recovered *via* centrifugation after natural cooling to room temperature, washed with water three times and ethanol once, and was then dried in air at 70 ^{o}C for 24 h.

Chemical analysis. Elemental contents of the products were determined for Ln *via* inductively coupled plasma (ICP) spectroscopy (Model IRIS Advantage, Jarrell-Ash Japan, Kyoto, Japan), for N *via* spectrophotometry (Ubest-35, Japan Spectroscopic Co., Ltd, Tokyo), and for C and S *via* combustion-infrared absorptiometry (Model CS-444LS, LECO, St. Joseph, MI). The detection limit of the above analyses is 0.01 wt% in each case.

Powder X-ray diffraction. Phase characterization was performed *via* X-ray diffractometry (XRD, Model RIN T2200, Rigaku, Tokyo, Japan) under 40 kV/40 mA, using monochromatic Cu-*Kα* radiation (λ=0.15406 nm). The XRD data for Rietveld analysis were measured via the step-scan mode, with a step size of 0.02° and an

accumulation time of 35 s. Profile fitting, crystal structure searching and Rietveld refinements were performed using the TOPAS 4.2 software.[43]

Electron microscopy and electron diffraction. Product morphology was observed *via* field-emission scanning electron microscopy under an acceleration voltage of 10 kV (FE-SEM, Model S-5000, Hitachi, Tokyo). Selected area electron diffraction (SAED) and high-resolution lattice imaging were attained with a transmission electron microscope working at 200 kV (TEM, Model JEM-2100F, JOEL, Tokyo). The TEM sample was prepared by dispersing a small amount of sufficiently ground powder in ethanol via sonication, followed by depositing a few drops of the resultant suspension onto a carbon-coated grid and then air drying.

FTIR spectroscopy. Fourier transform infrared spectroscopy (FTIR, Model 4200, JASCO, Tokyo), performed by the standard KBr pellet method, was used to investigate the functional groups built in the compounds.

Thermolysis. Thermal decomposition of the layered compound was investigated *via* thermogravimetry/differential thermal analysis (TG/DTA, Model STA449F3, Jupiter, NETZSCH, Germany) in flowing simulated air (50 mL/min), with a constant heating rate of 10 ^{o}C/min in the wide temperature range of RT-1560 ^{o}C.

Derivation of $Ln_2O_2SO_4$ and Ln_2O_2S. The anhydrous $Ln_2(OH)_4SO_4$ was calcined in ambient air at 800 ^{o}C and in flowing H_2 (200 mL/min) at 900-1200 ^{o}C to produce $Ln_2O_2SO_4$ and Ln_2O_2S, respectively, with a holding time of 1 h at the annealing temperature and a heating rate of 5 ^{o}C/min in the ramp stage.

Photoluminescence. The excitation, emission and fluorescence decay kinetics were measured on an FP-6500 fluorospectrophotometer (JASCO, Tokyo) equipped with a 150 W xenon lamp for excitation, using a scan speed of 100 nm/min and a slit width of 3 nm for both excitation and emission.

■ RESULTS AND DISCUSSION

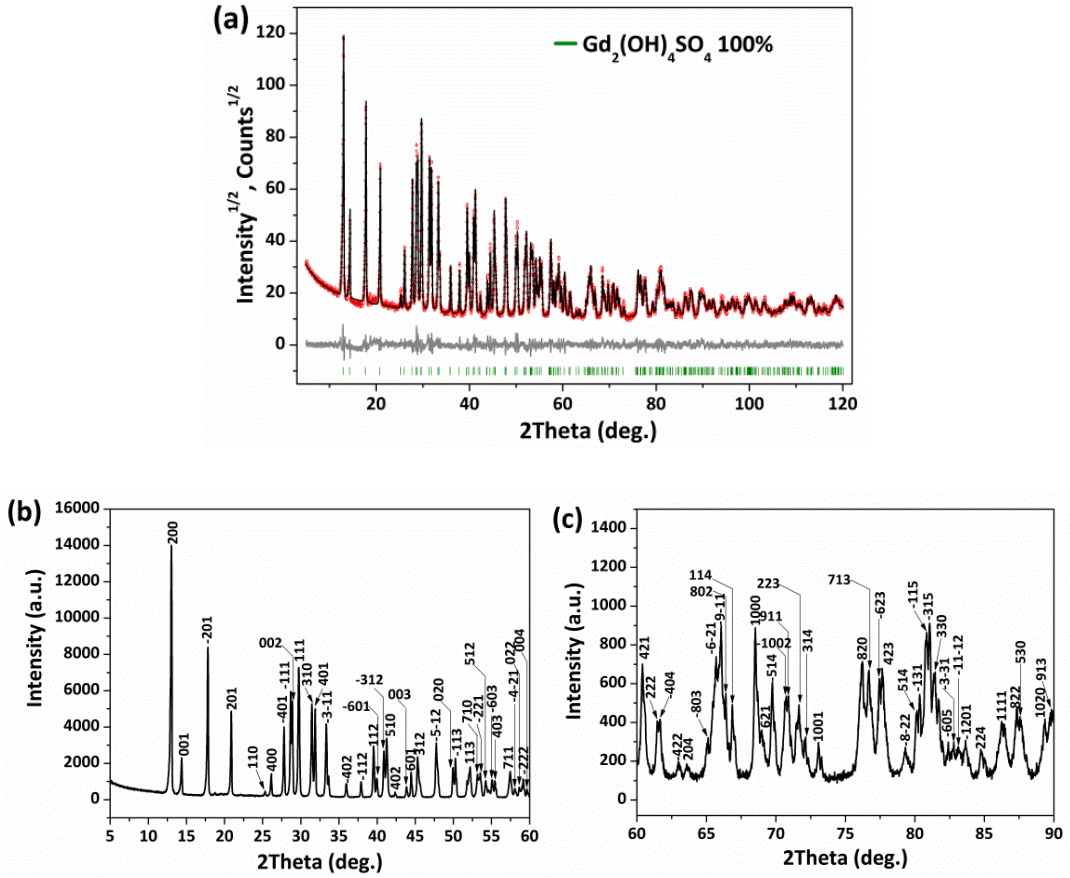

Figure 1. The final Rietveld difference plot of the $Gd_2(OH)_4SO_4$ compound obtained *via* hydrothermal reaction at 150 ^oC and pH=10 (a), and indexation of the diffraction peaks in the 2θ range of 5-60^o (b) and 60-90^o (c). In panel (a), the observed pattern is shown by the black solid line, the calculated data are shown by the red dots, the positions of Bragg reflections are indicated with the green tick marks, and the difference between the results of experiment and calculation is given by the gray line.

Characterization and structure analysis of $Gd_2(OH)_4SO_4$. Hydrothermal reaction of the turbid solution containing $Gd(NO_3)_3$, $(NH_4)_2SO_4$, and $NH_3{\cdot}H_2O$ at 150 ^oC and pH=10 produced a white precipitate. XRD analysis yielded sharp and symmetric reflections, indicating a highly crystalline nature of the product (Figure 1a). Elemental analysis of the same product found ~66.6 wt% of Gd, 6.90 wt% of S, 0.01 wt% of N, and 0.06 wt% of C, from which the chemical formula of

$Gd_2(OH)_{3.91}(SO_4)_{1.01}(NO_3)_{0.003}(CO_3)_{0.02}$ was derived if one assumes that the trace amounts of N and C solely came from the contamination of NO_3^- (from Gd nitrate) and CO_3^{2-} (from the dissolved atmospheric CO_2). The product can accordingly be approximated as $Gd_2(OH)_4SO_4$. This composition is identical to that of the recently reported LRH of $Gd_2(OH)_4SO_4 \cdot 2H_2O$,[29,42] except that it does not contain any hydration water. The absence of crystal water was further confirmed by comparing the FTIR responses of this new compound and $Ln_2(OH)_4SO_4 \cdot 2H_2O$ (Figure S1), where it is clearly seen that they both contain hydroxyls and SO_4^{2-}, but the former lacks the O-H stretching (ν_1 and ν_3, ~3219 cm^{-1}) and H-O-H bending (ν_2, ~1676 cm^{-1}) vibrations of hydration water.

Crystal structure decipherment found that all the XRD peaks of $Gd_2(OH)_4SO_4$ can be indexed by the *C*-centered monoclinic cell, and further analysis of reflection extinction showed that the most probable space group is *C*2/*m*. In order to establish the crystal structure a simulated annealing procedure was applied to the randomized coordinates of one Gd, one S and four O ions.[44] Eighteen varied parameters were yielded, indicating the rationality and high rate of success of the proposed crystal structure. The dynamical occupancy correction of the atoms was used to merge the ions falling in a special position.[45-47] After the calculations, a solution was found with well-acceptable *R*-factors (Table 1). The proposed crystal structure contains one SO_4^{2-} tetrahedron disordered between two positions like in the hydrated LRH of $Ln_2(OH)_4SO_4 \cdot 2H_2O$,[29,30] and the LnO_9 polyhedron is in the form of three-caped trigonal prism with one O node disordered between two positions (Figure 2). Hydrogen

atoms were not localized in the difference electron map and their positions could not be derived from the analysis of probable hydrogen bonds, and therefore they are omitted in the crystal structure. Refinement of this model is stable and gives well-acceptable *R*-factors (Table 1). The fractional atomic coordinates, isotropic displacement parameter (Å^2), and atomic occupancy are shown in Table 2, and the main bond lengths of the structure can be found in Table S1. The structural analysis of $Gd_2(OH)_4SO_4$ using the program PLATON[48] did not reveal additional elements of symmetry, which further confirms the suggested *C*2/*m* space group. The diffraction peaks were thus indexed in Fig. 1b,c according to the results of Rietveld refinement.

Table 1. Results of structure refinements for the anhydrous hydroxyl sulfate compound of $Gd_2(OH)_4SO_4$

Sp.gr.	Cell parameters (Å), axis angle β (°), and cell volume V (Å^3)	R_{wp}, R_p (%), χ^2	R_B (%)
*C*2/*m*	a = 13.8759 (5) b = 3.6577 (1) c = 6.2842 (2) β = 99.057 (1) V = 314.97 (2)	9.31, 4.70, 1.98	2.95

Table 2. Fractional atomic coordinates, isotropic displacement parameters B_{iso} (Å^2), and atomic occupancy (Occ.) of $Gd_2(OH)_4SO_4$

	x	*y*	*z*	B_{iso}	Occ.
Gd	0.19468 (7)	0.5	0.2303 (2)	0.95 (8)	1
S	0.5006 (7)	0.5	0.131 (1)	1.5 (2)	0.5
O_{1h}	0.1690 (6)	0	0.480 (2)	2.0 (3)	1
O_{2h}	0.2938 (6)	0	0.152 (1)	2.0 (3)	1
O_3	0.5869 (7)	0.5	0.049 (2)	3.3 (3)	1
O_4	0.5021 (7)	0.188 (3)	0.723 (1)	2.3 (3)	0.5

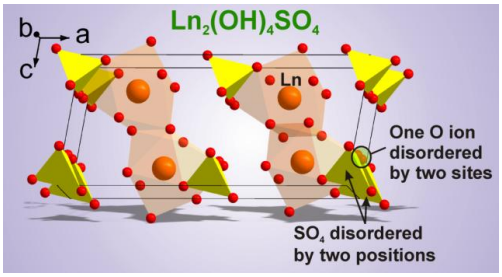

Figure 2. Schematic illustration of the crystal structure of $Gd_2(OH)_4SO_4$.

Figure 2 shows the deciphered crystal structure of anhydrous $Gd_2(OH)_4SO_4$ (space group: *C*2/*m*), which can be viewed as an alternative stacking of the sulfate anion and hydroxide main layer, composed of [GdO_9] polyhedra, along the *a*-axis. Among the nine O atoms coordinated to each Gd center, six are stemming from hydroxyls and three from the SO_4^{2-} tetrahedron, and the [GdO_9] polyhedron presents three-capped trigonal prism in the structure. Each unit cell contains four Gd atoms, and thus the structural composition can be expressed as $Gd_4(OH)_8(SO_4)_2$. The circle shows that one O ion is disordered by two sites (one O ion distributed over these two sites). The reason for such a behavior is due to the same potential energy and small potential barrier of these two sites, which allows the O ion easily jumps from one site to another as shown in Figure S2. Averaging over time and space leads to "two sites" occupied by one O ion with occupancy of 1/2 for each. This can be understood as (1) one O ion jumps from one site to another site (disordering over time), and (2) one O ion is located in a first site in one unit cell, but another O ion is located in a second site in another unit cell (disordering over space). Though it cannot be credibly decided which type of disordering happens in the structure, such disordering usually occurs in a structure with large voids in which the ion can easily migrate.

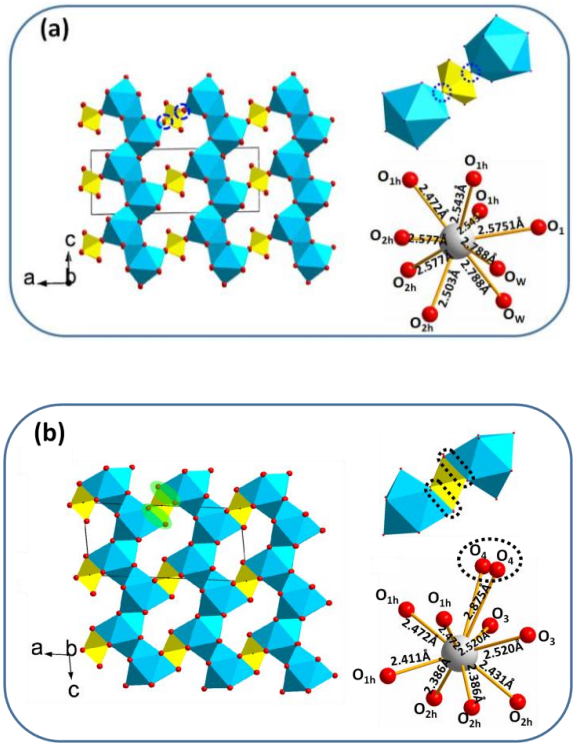

Figure 3. A Comparison of the crystal structures of $Gd_2(OH)_4SO_4{\cdot}2H_2O$ (a) and $Gd_2(OH)_4SO_4$ (b).

Figure 3 compares the stacking and coordination modes of the anhydrous $Gd_2(OH)_4SO_4$ (Figure 3b) and its hydrated $Gd_2(OH)_4SO_4{\cdot}2H_2O$ counterpart (Figure 3a). The two structures share similarities in that the Gd-containing main layer and inter-layer SO_4^{2-} stack along the *a*-axis and that the host layer solely consists of [GdO_9] polyhedra. It should be noted that Figure 3b shows CN=10 because a static averaged structure was given for the disordered O atom (O_4) as discussed earlier. Despite the above structural similarities, the $Gd_2(OH)_4SO_4$ anhydrous LRH distinguishes itself from $Gd_2(OH)_4SO_4{\cdot}2H_2O$ in that: (1) the hydroxide main layers are linked with the inter-layer anion through sharing edges (Figure 3b) rather than "O" node (Figure 3a) of the sulfate tetrahedron; (2) in $Gd_2(OH)_4SO_4{\cdot}2H_2O$, among the nine O atoms coordinated to each Gd center, six are stemming from hydroxyls, two from H_2O molecules and one from SO_4^{2-} tetrahedron, while in $Gd_2(OH)_4SO_4$, six are from

hydroxyls and three from the SO_4^{2-} group, though the [GdO_9] similarly presents as three-capped trigonal prism in both the structures; (3) $Gd_2(OH)_4SO_4$ shows a smaller gallery height (~6.85 Å) and cell volume (~314.97 $Å^3$) than $Gd_2(OH)_4SO_4 \cdot 2H_2O$ (gallery height ~8.32 Å; cell volume ~388.14 $Å^3$)[42] due to the absence of crystal water.

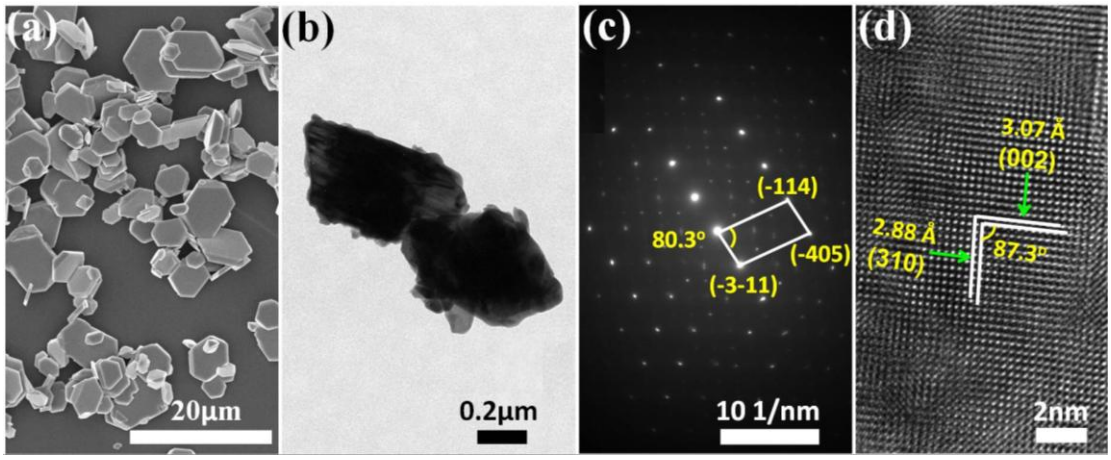

Figure 4. FE-SEM (a) and TEM (b) morphologies, SAED pattern (c), and HRTEM lattice fringes (d) for $Gd_2(OH)_4SO_4$.

FE-SEM observation found that the $Gd_2(OH)_4SO_4$ LRH crystallized as quasi-hexagons with the lateral sizes and thicknesses of up to ~10 and 1.5 μm, respectively (Figure 4a). SAED analysis (Figure 4c) of the crushed crystallites (Figure 4b) yielded well-arranged diffraction spots, indicating high crystallinity of the sample. The identified (-3-11), (-114), and (-405) diffractions have the *d*-spacings of ~2.78, 1.47, and 1.23 Å, respectively, which are in close vicinity to the values of $d_{(-3-11)}$=2.694, $d_{(-114)}$=1.442, and $d_{(-405)}$=1.231 Å derived from Rietveld refinement of the XRD pattern (Table S2). The (-3-11) and (-114) planes would have a dihedral angle of ~84.7°, as calculated from the lattice constants and axis angle (β) derived via Rietveld refinement (Table 1), and the value is indeed close to the ~80.3° observed

from the SAED pattern. HRTEM analysis (Figure 4d) well resolved the lattice fringes with interplanar distances of ~3.07 and 2.88 Å and a dihedral angle of ~87.3°, which can be well assigned to the (002) and (310) planes of monoclinic $Gd_2(OH)_4SO_4$, respectively, according to the results of Rietveld refinement ($d_{(002)}$=3.103 Å and $d_{(310)}$=2.855 Å in Table S2; calculated dihedral angle: ~84.1°). The well corresponding results of TEM analysis and Rietveld refinement further confirmed the crystal structure proposed in this work for the $Gd_2(OH)_4SO_4$ anhydrous LRH.

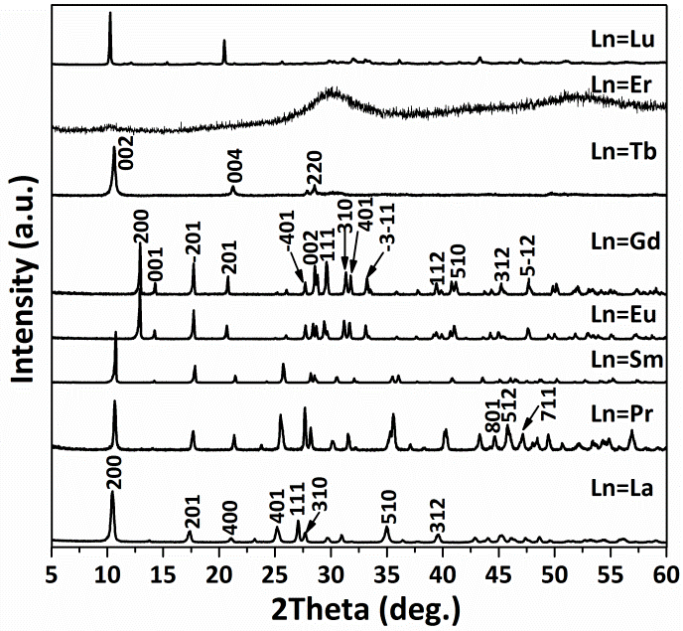

Figure 5. XRD patterns of the products obtained *via* hydrothermal reaction at 150 °C and pH=10 for the typical lanthanides (Ln) indicated in the figure.

Extended synthesis of $Ln_2(OH)_4SO_4$ anhydrous LRH. Under identical hydrothermal reaction at 150 °C and pH=10 for 24 h, the synthesis of $Ln_2(OH)_4SO_4$ anhydrous LRH was attempted for the full spectrum of lanthanides, and Figure 5 shows the XRD patterns of a series of representative products. It is seen that only $Eu_2(OH)_4SO_4$ can be obtained aside from the $Gd_2(OH)_4SO_4$ discussed above. The

La-Sm products conform well to the hydrated LRH of $Ln_2(OH)_4SO_4{\cdot}2H_2O$.[29,30,31] It is worth noting that Tb^{3+} (0.1095 nm for CN=9) is only slightly smaller than Gd^{3+} (0.1107 nm for CN=9), but its product crystallized as $Tb_2(OH)_5A{\cdot}nH_2O$,[15,32] instead of $Tb_2(OH)_4SO_4$, where the A group was inferred to be SO_4^{2-} from the FTIR response of the product (Figure S1). The Er-product exhibits an amorphous diffraction and appears to be a transient state between those of Tb and Lu, as similarly observed before during hydrothermal crystallization of $Ln_2(OH)_4SO_4{\cdot}2H_2O$ hydrated LRH.[42] The Lu-product cannot be indexed with any of the currently available JCPDS Card or reported reference. The results of elemental analysis (Table S3) and FTIR spectroscopy (Figure S1), however, indicated that it contains OH^- and SO_4^{2-} and has the nominal composition of $Lu_2(OH)_{4.95}(SO_4)_{0.38}(NO_3)_{0.14}(CO_3)_{0.08}{\cdot}1.04H_2O$, which is quite close to the aforementioned $Tb_2(OH)_5(SO_4)_{0.5}{\cdot}nH_2O$. Structure decipherment is yet unsuccessful for this Lu product. The different crystallization behaviors across the lanthanide spectrum were believed to be mainly caused by lanthanide contraction. The Ln^{3+} ion in an aqueous solution would present itself in the form of $[Ln(OH)_x(H_2O)_y(SO_4)_z]^{3-x-2z}$ complex,[49] where the OH^-, SO_4^{2-}, and H_2O species are expected to compete with each other to coordinate with Ln^{3+} and thus affect the final composition of the product. Under the same hydrothermal condition, the smaller ions of Tb-Lu would undergo a higher extent of hydrolysis (larger x while smaller z),[50] and therefore higher OH^-/Ln^{3+} (~2.5) molar ratios were observed for their products.

It can thus be inferred from the above that lowering the pH of the reaction system would favor the crystallization of $Ln_2(OH)_4SO_4$ anhydrous LRH, and indeed

phase-pure $Tb_2(OH)_4SO_4$ and $Dy_2(OH)_4SO_4$ were successfully produced at 150 ^oC under pH=9 and 8, respectively. The result is encouraging and directing, and further lowering the pH to 7 allowed the crystallization of $Ln_2(OH)_4SO_4$ at 150 ^oC for the smaller ions of Ho^{3+} (0.1072 nm for CN=9), Y^{3+} (0.1075 nm for CN=9) and Er^{3+} (0.1062 nm for CN=9). It is also interesting to find out that at the lowest applicable pH of 7 (no precipitation under even lower pH), phase pure $Ln_2(OH)_4SO_4$ can be successfully synthesized at the slightly higher temperature of 180 ^oC for the even smaller Tm^{3+} (0.1052 nm for CN=9) and Yb^{3+} (0.1042 nm for CN=9) and at 200 ^oC for the smallest Lu^{3+} (0.1032 nm for CN=9). The XRD patterns of these extended members of $Ln_2(OH)_4SO_4$ (Ln=Tb-Lu) are shown in Figure 6, and their chemical compositions were further confirmed by the results of FTIR spectroscopy (Figure S3) and elemental analysis (Table S4, for the typical Ln of Y and Lu). It is noteworthy that our extensive synthesis efforts indicated that the anhydrous LRH of $Ln_2(OH)_4SO_4$ is only obtainable for Ln=Eu-Lu (including Y). For the larger Ln ions of La^{3+}-Sm^{3+}, either raising the reaction temperature or lowering the solution pH would lead to the crystallization of anhydrous $Ln(OH)SO_4$ (SO_4/Ln=1:1 molar ratio). The above results thus clearly reveal that solution pH and reaction temperature decisively determine phase selection, and the optimal hydrothermal conditions vary with the type of Ln^{3+} owing to the different hydrolysis behaviors of Ln^{3+} by lanthanide contraction. It can also be inferred from the above results that either a lower pH or a higher reaction temperature facilitates SO_4^{2-} coordination to Ln^{3+} and meanwhile expels out the weakest coordinating H_2O molecules from the coordination sphere of Ln^{3+} to yield

anhydrous $Ln_2(OH)_4SO_4$.

SEM observation (Figure S4) revealed that the morphology of $Ln_2(OH)_4SO_4$ is closely related to the type of Ln and the hydrothermal conditions. The Eu, Gd and Tb products, synthesized at the relatively high pH of 10 and 9, are quasi-hexagonal microplates (Figure S4), while the Dy-Lu products, obtained at the lower pH of 8 and 7, are aggregated microspheres or irregular shapes (Figure S4). The aggregation under lower pH was believed to be caused by attraction of the negatively charged SO_4^{2-} groups by surface adsorbed protons. The different morphologies and dimensions of the particles/crystallites may largely account for the varying relative intensities of XRD peaks, for example (200) and (002), for different Ln (Figure 6).

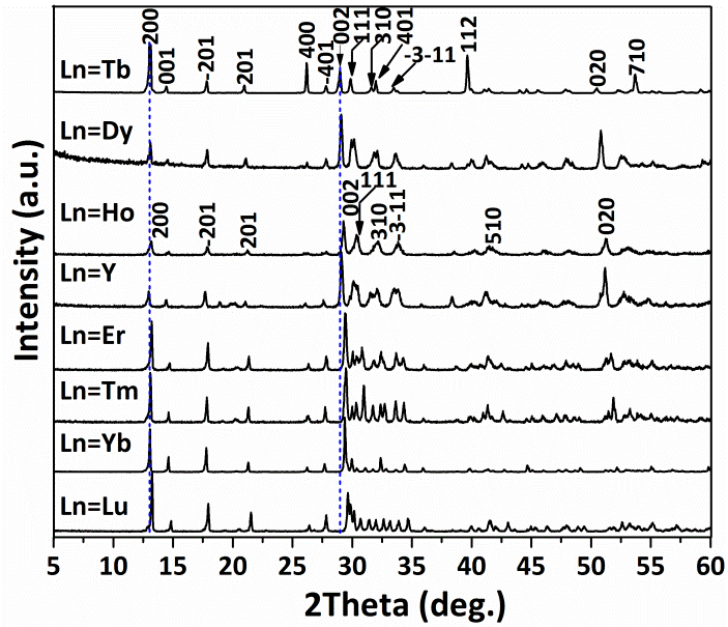

Figure 6. XRD patterns of the extended members of $Ln_2(OH)_4SO_4$ (Ln=Tb-Lu and Y), with the hydrothermal conditions summarized in Table S5 for each sample.

With the structure model solved for $Gd_2(OH)_4SO_4$, the cell parameters of $Ln_2(OH)_4SO_4$ were derived *via* pattern fitting and the results are tabulated in Table S6

and also exhibited in Figure 7 as a function of the ionic radius of Ln^{3+}. It is seen that the lattice constants (*a*, *b*, and *c*; Figure 7a-c) and cell volume (*V*; Figure 7d) tend to successively decrease for a smaller Ln^{3+}, conforming to lanthanide contraction, while the axis angle β behaves oppositely (Figure 7e). It was also noticed that the *b* and *c* parameters show slopes of ~1.625 and 1.052 with decreasing Ln^{3+} size from Eu^{3+} to Lu^{3+}, respectively, while the *a* parameter declines to a much lesser extent and with a slope of only ~0.395. The (0*kl*) and (*h*00) diffractions reflect structural features of the host layers and the stacking of the host layer along the *a*-axis, respectively. Shrinkage of the *a* dimension is thus significantly constrained by the rigidly pillaring SO_4^{2-} because the interlayer SO_4^{2-} rarely shows substantial distortion from the regular tetrahedron in most crystal structures. The limited contraction of the *a* parameter corresponds well with the almost non-shifting (*h*00) peaks (such as 200; Figure 6).

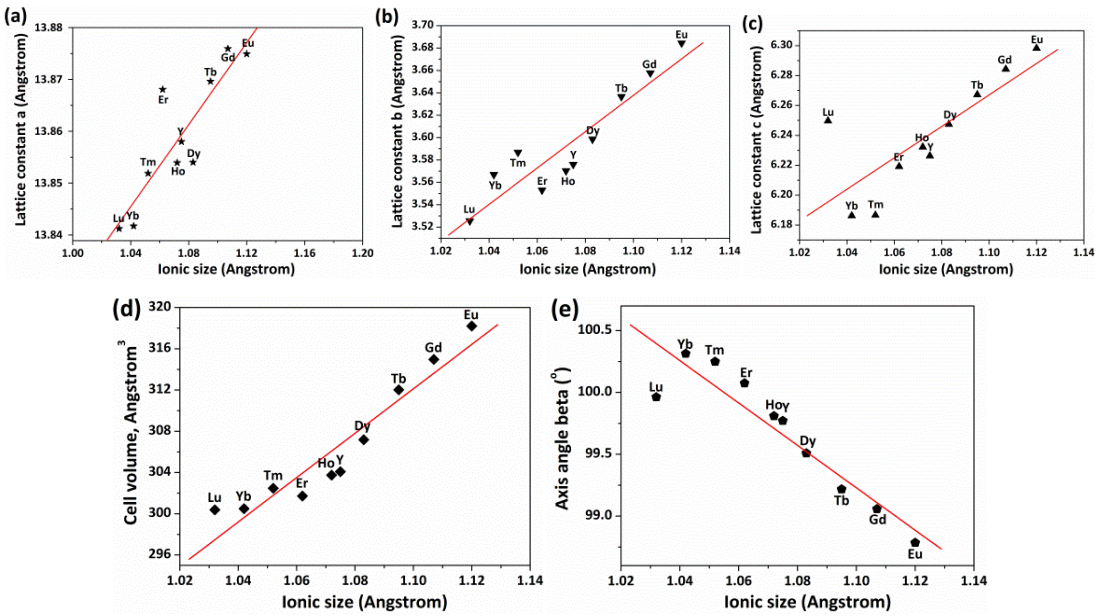

Figure 7. Correlation of lattice parameters *a* (part a), *b* (part b), and *c* (part c), cell volume *V* (part d), and axis angle β (part e) with the ionic radius of Ln^{3+} for $Ln_2(OH)_4SO_4$ (Ln=Eu-Lu and Y). The ionic radius for 9-fold coordinated Ln^{3+} is cited from reference 51.

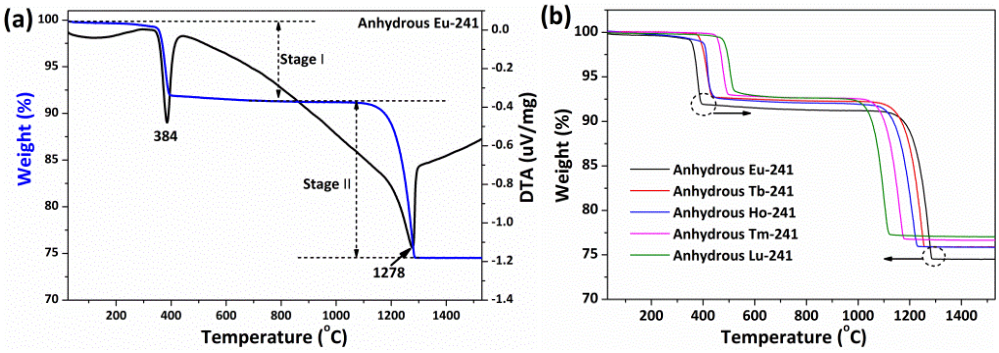

Figure 8. The TG/DTA curves for $Eu_2(OH)_4SO_4$ (a) and a comparison of the TG curves for some representative $Ln_2(OH)_4SO_4$ anhydrous compounds (b).

Table 4. Data of thermal decomposition for the $Ln_2(OH)_4SO_4$ anhydrous LRH in simulated air (Ln=Eu-Lu and Y)

Ln	Peak 1 (°C)	Peak 2 (°C)	Temperature range for $Ln_2O_2SO_4$ (°C)	Weight loss I (%)	Weight loss II (%)
Eu	384	1278	437-1125	8.62	16.93
Gd	415	1270	471-1123	8.16	16.71
Tb	422	1249	479-1086	7.62	16.51
Dy	450	1264	505-1098	7.71	16.57
Ho	420	1215	491-1066	7.84	16.31
Y	430	1208	503-1057	11.27	23.50
Er	461	1192	523-1051	8.93	16.07
Tm	483	1167	539-1024	7.24	16.09
Yb	502	1118	557-980	7.11	15.69
Lu	508	1104	565-978	7.32	15.61

Thermolysis. The thermal decomposition of $Ln_2(OH)_4SO_4$ (Ln=Eu-Lu, and Y) has been investigated *via* DTA/TG in simulated air for the wide temperature range of RT-1560 °C. The results of $Eu_2(OH)_4SO_4$ are shown in Figure 8a for example, and the rest can be found in Figure S5. Compared with its hydrated $Eu(OH)_4SO_4{\cdot}2H_2O$ counterpart (Figure S6), a distinct feature of $Eu_2(OH)_4SO_4$ is that it lacks the stage of dehydration up to ~300 °C (~7.7% of weight loss accompanied by an endotherm at ~269 °C, Figure S6), which again confirms the anhydrous nature of $Eu_2(OH)_4SO_4$. The $Ln_2(OH)_4SO_4$ compounds synthesized in this work similarly show two steps of

weight losses that correspond to dehydroxylation (up to ~550 °C) and desulfurization (above ~1000 °C) to yield $Ln_2O_2SO_4$ and Ln_2O_3, respectively (Figure 8). The reactions of the two stages can accordingly be expressed as $Ln_2(OH)_4SO_4 \rightarrow Ln_2O_2SO_4 + 2H_2O$ (stage I) and $Ln_2O_2SO_4 \rightarrow Ln_2O_3 + SO_3$ (stage II). The well corresponding observed (Table 4) and theoretical (Table S7) weight losses of each stage further confirm the proposed decomposition procedure. The occurrence temperature of each stage nonetheless shows clear dependence on the type of Ln. As shown in Figure 8b and Table 4, dehydroxylation occurs towards a higher temperature for a smaller Ln^{3+} while desulfuration behaves oppositely. The temperature range of $Ln_2O_2SO_4$ existence thus narrows towards a smaller Ln^{3+}, which makes $Lu_2O_2SO_4$ the least stable amongst the $Ln_2O_2SO_4$ family.

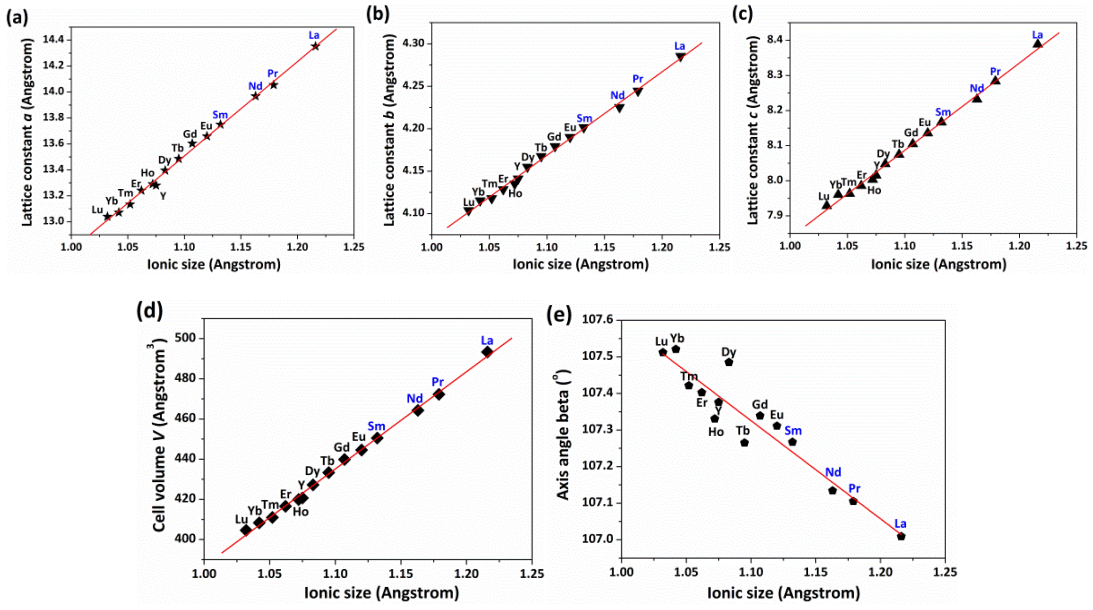

Figure 9. Correlation of lattice parameters *a* (part a), *b* (part b) and *c* (part c), cell volume *V* (part d), and axis angle *β* (part e) with the ionic radius of Ln^{3+} for $Ln_2O_2SO_4$. The ionic radius of Ln^{3+} and the structural data for Ln=La-Sm (blue colored) are taken from references 51 and 42, respectively.

Green derivation of $Ln_2O_2SO_4$ and Ln_2O_2S. According to the results of TG (Figure 8b), calcining $Ln_2(OH)_4SO_4$ in air at 800 ^oC for 1 h yielded $Ln_2O_2SO_4$ in a phase-pure form (Figure S7). The group of oxysulfate compounds crystallize in the monoclinic system (space group: *C*2/*c*), in which each Ln is bonded with seven oxygen atoms (three from SO_4^{2-}) to make one-capped trigonal prism.[31] The diffraction peaks of $Ln_2O_2SO_4$ clearly shift to larger 2θ angles for a smaller Ln^{3+}, in compliance with lanthanide contraction. The $Ln_2(OH)_4SO_4$ anhydrous LRH newly discovered in this work (Ln=Eu-Lu and Y), together with the $Ln_2(OH)_4SO_4{\cdot}2H_2O$ hydrated LRH reported recently (Ln=La-Dy),[42] allows for the first time the green synthesis of $Ln_2(OH)_4SO_4$ for the full spectrum of lanthanides (excluding Ce^{3+} and Pm^{3+}). Figure 9 exhibits structural parameters of the $Ln_2O_2SO_4$ derived from $Ln_2(OH)_4SO_4$ (Ln=Eu-Lu and Y) and $Ln_2(OH)_4SO_4{\cdot}2H_2O$ (Ln=La-Sm),[42] where it is seen that the lattice constants (Figure 9a-c) and cell volume (Figure 9d) linearly decrease toward a smaller Ln^{3+} while an opposite trend was observed for the axis angle β (Figure 9e).

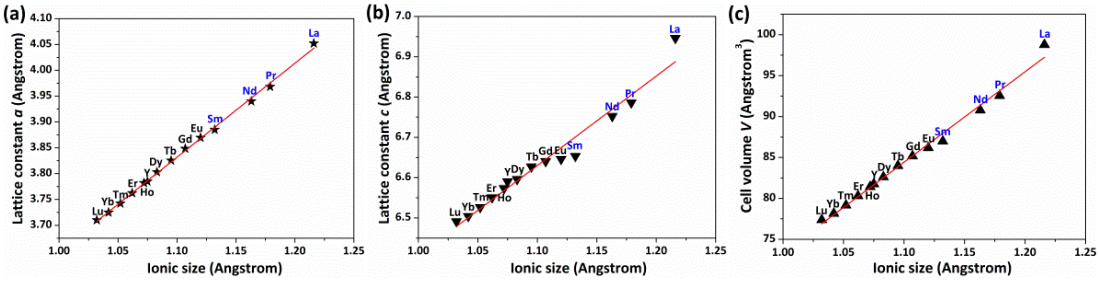

Figure 10. Correlation of the lattice parameters *a* (part a) and *c* (part b) and cell volume *V* (part c) with the ionic radius of Ln^{3+} for Ln_2O_2S. The ionic radius of Ln^{3+} and the structural data for Ln=La-Sm are taken from references 51 and 42, respectively.

Treating $Ln_2(OH)_4SO_4$ in hydrogen may allow dehydroxylation and reduction of the S^{6+} in SO_4^{2-} to S^{2-} and thus the formation of Ln_2O_2S. Considering that the reducing

power of H_2 is yet rather low at the dehydration temperature (up to ~550 ^oC, Figure 8b), Ln_2O_2S was thus expected to form *via* the sequential reactions of $Ln_2(OH)_4SO_4$ → $Ln_2O_2SO_4$ + $2H_2O$ (dehydroxylation) and $Ln_2O_2SO_4$ +$4H_2$ → Ln_2O_2S + $4H_2O$ (reduction). The XRD patterns of the products calcined from $Ln_2(OH)_4SO_4$ in flowing H_2 at 1200 ^oC for 1 h are shown in Figure S8. It is seen that the Eu and Gd products can be well indexed to single-phased Ln_2O_2S of a hexagonal structure. The oxysulfide compounds belong to the *P*-3*m*1 space group, where Ln is bonded with three sulfur and four oxygen atoms to make mono-capped polyhedron of seven-fold coordination.[31] Cubic-structured Ln_2O_3 impurity was unexpectedly found for the products of smaller Ln^{3+} (Ln=Tb-Eu and Y), as indicated with an asterisk for the (222) diffraction in each case. Rietveld refinement found that the portion of Ln_2O_3 gradually increases towards a smaller Ln^{3+}, from ~3.3 wt% for Tb^{3+} to ~78.5 wt% for Lu^{3+}. The phase constituents and cell parameters determined via Rietveld analysis for Ln_2O_2S and Ln_2O_3 can be found in Table S8. It should be noted that calcining $Ln_2(OH)_4SO_4$ at the lower temperature of 900 ^oC yielded similar XRD results, though at which the reducing powder of H_2 is known to be well acceptable and $Ln_2O_2SO_4$ would be stable in air (Figure 8b and Table 4). The above observations may thus reveal that the affinity of SO_4^{2-} towards Ln^{3+} is significantly lower in H_2 than in air. As a result, the S could have partially dissociated as SO_x upon calcining the $Ln_2(OH)_4SO_4$ of Ln=Tb-Lu (including Y) in H_2. The gradually decreasing thermal stability of $Ln_2O_2SO_4$ (Figure 8b and Table 4) well explains the increasing content of Ln_2O_3 in the reduction product for a smaller Ln^{3+} (Table S8). Figure 10 depicts the influence of Ln^{3+} size on the

structural parameters of Ln_2O_2S for the full spectrum of lanthanides, where it is seen that the lattice constants (*a* and *c*, Figure 10a,b) and cell volume (Figure 10c) almost linearly decrease towards a smaller Ln^{3+}.

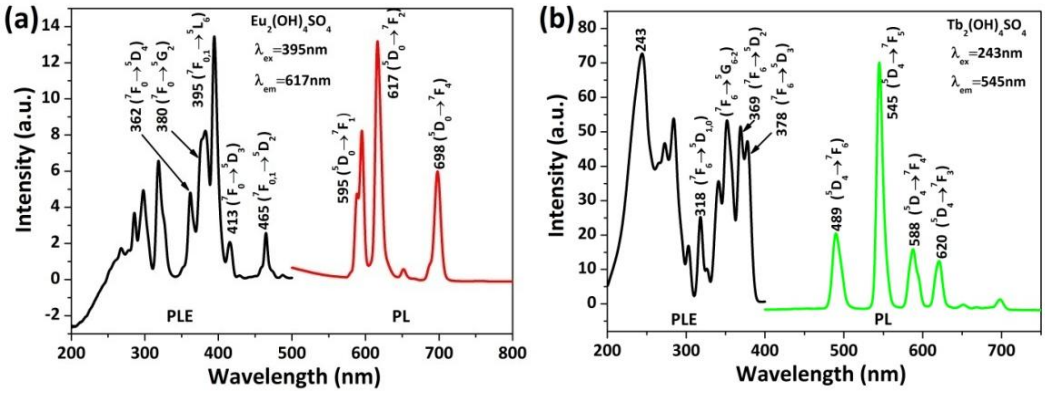

Figure 11. PLE (black lines) and PL (colored lines) spectra of $Eu_2(OH)_4SO_4$ (a) and $Tb_2(OH)_4SO_4$ (b), with the excitation and emission wavelengths used for the measurements included.

Photoluminescent properties. Photoluminescence investigation indicated that the $Eu_2(OH)_4SO_4$ and $Tb_2(OH)_4SO_4$ LRH compounds produce red and green emissions through their characteristic *f-f* transitions under UV excitation, and the excitation (PLE) and emission (PL) spectra are shown in Figure 11. It is noteworthy that the other optically active ions of Gd^{3+}, Dy^{3+}, Ho^{3+}, Er^{3+}, and Tm^{3+} exhibit negligible luminescence in the $Ln_2(OH)_4SO_4$ lattice. The PLE spectrum of $Eu_2(OH)_4SO_4$ (λ_{em}=617 nm) shows sharp excitation peaks ascribable to the intra-$4f^6$ transitions of Eu^{3+}, with the $^7F_0 \rightarrow {}^5L_6$ transition at 395 nm being the strongest (Figure 11a). Under the excitation of 395 nm, the $^5D_0 \rightarrow {}^7F_J$ transitions of Eu^{3+} were observed with the $^5D_0 \rightarrow {}^7F_2$ (617 nm) red emission being the most prominent (Figure 11a). This conforms to the low site symmetry of Eu^{3+} in the monoclinic lattice. The excitation spectrum of $Tb_2(OH)_4SO_4$ (λ_{em}=545 nm) is composed of the $4f^8 \rightarrow 4f^7 5d^1$ inter-configurational

transitions and the intra-$4f^8$ transitions in the ~200-300 and 300-400 nm spectral regions, respectively, with the former being dominant (Figure 11b). Under excitation with the spin-allowed *f-d* transition at 243 nm, the typical $^5D_4 \rightarrow {}^7F_J$ (J=3-6) transitions of Tb^{3+} were produced, with the $^5D_4 \rightarrow {}^7F_5$ green emission at 545 nm being predominant (Figure 11b). The fluorescence decay kinetics of the 617 nm red emission of $Eu_2(OH)_4SO_4$ (λ_{ex}=395 nm) and the 545 nm green emission of $Tb_2(OH)_4SO_4$ (λ_{ex}=243 nm) can both be fitted with a single exponential (Figure S9), from which the lifetime values of 0.67 and 0.78 ms were determined for the two compounds, respectively. The CIE chromaticity coordinates derived from the emission spectra are around (0.60, 0.39) and (0.36, 0.55) for $Eu_2(OH)_4SO_4$ and $Tb_2(OH)_4SO_4$, corresponding to orange red and yellowish green colors, respectively (Figure S10).

■ CONCLUSIONS

The anhydrous hydroxyl sulfate of $Ln_2(OH)_4SO_4$ (Ln=Eu-Lu and Y) has been hydrothermally synthesized in this work as a new family of layered rare-earth hydroxide *via* manipulating the coordination of Ln^{3+} center ion. It was generally observed that a higher reaction temperature and/or a lower solution pH favors the crystallization of $Ln_2(OH)_4SO_4$ for a smaller Ln^{3+}. Detailed analyses of the compounds in terms of crystal structure, thermal behavior, phase transformation to $Ln_2O_2SO_4$ and Ln_2O_2S, and photoluminescence have led to the following main conclusions: (1) $Ln_2(OH)_4SO_4$ crystallizes in the monoclinic system (space group: *C*2/*m*), with the structure built up *via* alternative stacking of the interlayer SO_4^{2-} and the two-dimensional host layers, composed of [LnO_9] polyhedra, along the *a*-axis. The

[LnO_9] polyhedron presents as three-capped trigonal prism and the host layers are linked together *via* edging sharing with SO_4^{2-} tetrahedron. $Ln_2(OH)_4SO_4$ shows a smaller gallery height and cell volume than its hydrated $Ln_2(OH)_4SO_4 \cdot 2H_2O$ counterpart due to the absence of crystal water; (2) The lattice parameters (*a*, *b*, *c*) and cell volume tend to decrease towards a smaller Ln^{3+} across the lanthanide series while an opposite trend was found for the axis angle *β*. The *a* parameter shows significantly smaller contraction than the *b* and *c* parameters with decreasing Ln^{3+} size due to the rigid pillaring of interlayer SO_4^{2-}; (3) $Ln_2(OH)_4SO_4$ undergoes dehydroxylation and then desulfurization to yield $Ln_2O_2SO_4$ and finally Ln_2O_3 in air. Dehydroxylation happens at a higher temperature towards a smaller Ln^{3+} while desulfurization behaves oppositely. As a consequence, the temperature window of $Ln_2O_2SO_4$ existence narrows towards a smaller Ln^{3+}; (4) Calcining $Ln_2(OH)_4SO_4$ in air at 800 °C yielded single-phased monoclinic $Ln_2O_2SO_4$ for Ln=Eu-Lu (including Y), whose lattice constants (*a*, *b*, *c*) and cell volume almost linearly decrease while the axis angle increases towards a smaller Ln^{3+}. Calcining $Ln_2(OH)_4SO_4$ in H_2 at 900-1200 °C only produced hexagonal structured Eu_2O_2S and Gd_2O_2S as pure phases. The product of the smaller Ln^{3+} (Ln=Tb-Lu and Y) is a phase mixture of Ln_2O_2S and Ln_2O_3, whose Ln_2O_3 content increases with decreasing radius of Ln^{3+}; (5) $Eu_2(OH)_4SO_4$ and $Tb_2(OH)_4SO_4$ exhibit orange red [chromaticity coordinates: (0.60, 0.39)] and yellowish green [chromaticity coordinates: (0.36, 0.55)] emissions under UV excitation at 395 and 243 nm, respectively. The 617 nm Eu^{3+} and 545 nm Tb^{3+} emissions were analyzed to have the fluorescence lifetimes of ~0.67 and 0.78 ms, respectively.

■ ASSOCIATED CONTENT

Supporting Information

The Supporting Information is available free of charge on the ACS Publications website.

Supporting figures and tables (PDF)

Crystallographic information files (cif)

Checkcif file (PDF)

Further details of the crystal structures $Gd_2(OH)_4SO_4$, may be obtained from Fachinformationszentrum Karlsruhe, 76344 Eggenstein-Leopoldshafen, Germany (fax: (+49)7247-808-666; E-mail: crystdata@fiz-karlsruhe.de; http://www.fiz-karlsruhe.de/request_for_deposited_data.html on quoting the deposition numbers: CSD-433211.

■ AUTHOR INFORMATION

Corresponding Authors

*(X.J.W.) E-mail: wangxuejiao@bhu.edu.cn

*(J.-G.L.) E-mail: li.jiguang@nims.go.jp

ORCID

Ji-Guang Li: 0000-0002-5625-7361

Author contributions

X.J.W., M.S.M. and J.-G.L. contributed equally to this work. All the authors were involved in the results discussion and have read and approved this final version.

Notes

The authors declare no competing financial interest.

■ ACKNOWLEDGMENTS

This work is supported in part by the National Natural Science Foundation of China (Grants No. 51672039) and the Russian Foundation for Basic Research (17-52-53031). Xuejiao Wang acknowledges the financial support from the China Scholarship Council for her overseas Ph. D. study (Contract No. 201406080035).

■ REFERENCES

(1) Junseok, L.; Jinhwan, K.; Won, J. K. Photothermally Controllable Cytosolic Drug Delivery Based On Core-Shell MoS_2-Porous Silica Nanoplates. *Chem. Mater.* **2016**, 28, 6417-6424.

(2) Zhang, W. P.; Xiao, X. Y.; Li, Y.; Zeng, X. Y.; Zheng, L. L.; Wan, C. X. Liquid-exfoliation of Layered MoS_2 for Enhancing Photocatalytic Activity of TiO_2/g-C_3N_4 Photocatalyst and DFT Study. *Appl. Surf. Sci.* **2016**, 389, 496-506.

(3) Gu, Y.; Lu, Z.; Chang, Z.; Liu, J.; Lei, X.; Li, Y.; Sun, X. NiTi Layered Double Hydroxide Thin Films for Advanced Pseudocapacitor Electrodes. *J. Mater. Chem. A.* **2013**, 1, 10655-10661.

(4) Liu, G. M.; Chen, J. P.; Yang, J. P.; Chen, G. M. Preparation and Characterization of Poly(vinylchloride)/Layered Double Hydroxide Nanocomposites with Enhanced Thermal Stability. *Polymer.* **2008**, 49, 3923-3927.

(5) Hu, Z. Q.; Chen, G. M. Novel Nanocomposite Hydrogels Consisting of Layered Double Hydroxide with Ultrahigh Tensibility and Hierarchical Porous Structure at Low Inorganic Content. *Adv. Mater.* **2014**, 26, 5950-5956.

(6) Cao, T. C.; Xu, K. L.; Chen, G. M.; Guo, C.-Y. Poly (ethylene terephthalate) Nanocomposites with a Strong UV-Shielding Function using UV-absorber Intercalated Layered Double Hydroxides. *RSC Adv.* **2013**, 3, 6282-6285.

(7) Zhang, Z.; Chen, G. M.; Liu, J. G. Tunable Photoluminescence of Europium-Doped Layered Double Hydroxides Intercalated by Coumarin-3-Carboxylate. *RSC Adv.* **2014**, 4, 7991-7997.

(8) Gandara, F.; Perles, J.; Snejko, N.; Iglesias, M.; Gomez-Lor, B.; Gutierrez-Puebla, E.; Monge, M. A. Layered Rare-Earth Hydroxides: A Class of Pillared Crystalline Compounds for Intercalation Chemistry. *Angew. Chem. Int. Ed.* **2006**, 45, 7998-8001.

(9) McIntyre, L. J.; Jackson, L. K.; Fogg, A. M. $Ln_2(OH)_5NO_3{\cdot}xH_2O$ (Ln=Y, Gd-Lu): A Novel Family of Anion Exchange Intercalation Hosts. *Chem. Mater.* **2008**, 20, 335-340.

(10) McIntyre, L. J.; Prior, T. J.; Fogg, A. M. Observation and Isolation of Layered and Framework Ytterbium Hydroxide Phases Using In Situ Energy-Dispersive X-ray Diffraction. *Chem. Mater.* **2010**, 22, 2635-2645.

(11) Song, Y. X.; Luo, M.; Lin, C. S.; Ye, N. Structural Modulation of Nitrate Group with Cations to Affect SHG Responses in $RE(OH)_2NO_3$ (RE = La, Y, and Gd): New Polar Materials with Large NLO Effect after Adjusting pH Values of Reaction Systems. *Chem. Mater.* **2017**, 29, 896-903.

(12) Carter, F. L.; Levinson, S. Hydrothermal Preparation, Single-crystal Lattice Parameters, and Decomposition Data for some Lathanide Dihydroxy Chlorides and the Related Hydroxy Chloride, $Yb_3O(OH)_5Cl_2$. *Inorg. Chem.* **1969**, 8, 2788-2791.

(13) Hashchke, J. M. Preparation, Phase Equilibria, Crystal Chemistry, and some Properties of Lanthanide Hydroxide Nitrates. *Inorg. Chem.* **1974**, 13, 1812-1818.

(14) Yapryntsev, A. D.; Baranchikov, A. E.; Skogareva, L. S.; Goldt, A. E.; Stolyarov, I. P.; Ivanova, O. S.; Kozik, V. V.; Ivanov, V. K. High-Yield Microwave Synthesis of Layered $Y_2(OH)_5NO_3{\cdot}xH_2O$ Materials. *CrystEngComm.* **2015**, 17, 2667-2674.

(15) Wu, X. L.; Li, J.-G.; Zhu, Q.; Liu, W. G.; Li, J.; Li, X. D.; Sun, X. D.; Sakka, Y. One-Step Freezing Temperature Crystallization of Layered Rare-Earth Hydroxide ($Ln_2(OH)_5NO_3{\cdot}nH_2O$) Nanosheets for a Wide Spectrum of Ln (Ln=Pr-Er, and Y), Anion Exchange with Fluorine and Sulfate, and Microscopic Coordination Probed *via* Photoluminescence. *J. Mater. Chem. C* **2015**, 3, 3428-3437.

(16) Kim, H.; Lee, B. I.; Jeong, H.; Byeon, S. H. Relationship Between Interlayer Anions and Photoluminescence of Layered Rare Earth Hydroxides. *J. Mater. Chem. C* **2015**, 3, 7437-7445.

(17) McIntyre, L. J.; Jackson, L. K.; Fogg, A. M. Synthesis and Anion Exchange Chemistry of New Intercalation Hosts Containing Lanthanide Cations, $Ln_2(OH)_5(NO_3){\cdot}xH_2O$ (Ln=Y, Gd-Lu). *J. Phys. Chem. Solids* **2008**, 69, 1070-1074.

(18) Geng, F. X.; Matsushita, Y.; Ma, R. Z.; Xin, H.; Tanaka, M.; Izumi, F.; Iyi, N.; Sasaki, T. General Synthesis and Structural Evolution of a Layered Family of

$Ln_8(OH)_{20}Cl_4{\cdot}nH_2O$ (Ln=Nd, Sm, Eu, Gd, Tb, Dy, Ho, Er, Tm, and Y). *J. Am. Chem. Soc.* **2008**, 130, 16344-16350.

(19) Poudret, L.; Prior, T. J.; McIntyre, L. J.; Fogg, A. M. Synthesis and Crystal Structures of New Lanthanide Hydroxyhalide Anion Exchange Materials, $Ln_2(OH)_5X{\cdot}1.5H_2O$ (X=Cl, Br; Ln=Y, Dy, Er, Yb). *Chem. Mater.* **2008**, 20, 7447-7453.

(20) Geng, F. X.; Xin, H.; Matsushita, Y.; Ma, R. Z.; Tanaka, M.; Izumi, F.; Iyi, N.; Sasaki, T. New Layered Rare-Earth Hydroxides with Anion-Exchange Properties. *Chem. Eur. J.* **2008**, 14, 9255-9260.

(21) Zhu, Q.; Li, J.-G.; Li, X. D.; Sun, X. D.; Qi, Y.; Zhu, M. Y.; Sakka, Y. Tens of Micron-Sized Unilamellar Nanosheets of Y/Eu Layered Rare-Earth Hydroxide: Efficient Exfoliation *via* Fast Anion Exchange and Their Self-Assembly into Oriented Oxide Film with Enhanced Photoluminescence. *Sci. Technol. Adv. Mater*. **2014**, 15, 014203.

(22) Hindocha, S. A.; McIntyre. L. J.; Fogg, A. M. Precipitation Synthesis of Lanthanide Hydroxyl Nitrate Anion Exchange Materials $Ln_2(OH)_5NO_3{\cdot}H_2O$ (Ln=Y, Eu–Er). *J. Solid State Chem.* **2009**, 182, 1070-1074.

(23) Liu, L. L.; Yu, M. H.; Zhang, J.; Wang, B. K.; Liu, W. S.; Tang, Y. Facile Fabrication of Color-Tunable and White Light Emitting Nano-Composite Films Based on Layered Rare-Earth Hydroxides. *J. Mater. Chem. C* **2015**, 3, 2326-2333.

(24) Jeong, H. J.; Lee, B.-I.; Byeon, S.-H. Antenna Effect on the Organic Spacer-Modified Eu-Doped Layered Gadolinium Hydroxide for the Detection of

Vanadate Ions over a Wide pH Range. *ACS Appl. Mater. Interfaces* **2016**, 8, 10946-10953.

(25) Xiang, Y.; Yu, X.-F.; He, D.-F.; Sun, Z. B.; Cao, Z. J.; Wang, Q.-Q. Synthesis of Highly Luminescent and Anion-Exchangeable Cerium-Doped Layered Yttrium Hydroxides for Sensing and Photofunctional Applications. *Adv. Funct. Mater.* **2011**, 21, 4388-4396.

(26) Geng, F. X.; Matsushita, Y.; Ma, R. Z.; Xin, H.; Tanaka, M.; Iyi, N.; Sasaki, T. Synthesis and Properties of Well-Crystallized Layered Rare-Earth Hydroxide Nitrates from Homogeneous Precipitation. *Inorg. Chem.* **2009**, 48, 6724-6730.

(27) Lee, K.-H.; Byeon, S.-H. Extended Members of the Layered Rare-Earth Hydroxides Family, $RE_2(OH)_5NO_3{\cdot}nH_2O$ (RE=Sm, Eu, and Gd): Synthesis and Anion-Exchange Behavior. *Eur. J. Inorg. Chem.* **2009**, 7, 929-936.

(28) Lee, K.-H.; Byeon, S.-H. Synthesis and Aqueous Colloidal Solutions of $RE_2(OH)_5NO_3{\cdot}nH_2O$ (RE=Nd and La). *Eur. J. Inorg. Chem.* **2009**, 31, 4727-4732.

(29) Liang, J. B.; Ma, R. Z.; Geng, F. X.; Ebina, Y.; Sasaki, T. $Ln_2(OH)_4SO_4{\cdot}nH_2O$ (Ln=Pr to Tb; n~2): A New Family of Layered Rare-Earth Hydroxides Rigidly Pillared by Sulfate Ions. *Chem. Mater.* **2010**, 22, 6001-6007.

(30) Geng, F. X.; Ma, R. Z.; Matsushita, Y.; Liang, J. B.; Michiue, Y.; Sasaki, T. Structural Study of a Series of Layered Rare-Earth Hydroxide Sulfates. *Inorg. Chem.* **2011**, 50, 6667-6672.

(31) Wang, X. J.; Li, J.-G.; Molokeev, M. S.; Zhu, Q.; Li, X. D.; Sun, X. D. Layered Hydroxyl Sulfate: Controlled Crystallization, Structure Analysis, and Green Derivation

of Multi-Color Luminescent $(La,RE)_2O_2SO_4$ and $(La,RE)_2O_2S$ Phosphors (RE=Pr, Sm, Eu, Tb, and Dy). *Chem. Eng. J.* **2016**, 302, 577-586.

(32) Wang, X. J.; Li, J.-G.; Zhu, Q.; Sun, X. D. Direct Crystallization of Sulfate-Type Layered Hydroxide, Derivation of $(Gd,Tb)_2O_3$ Green Phosphor, and Photoluminescence. *J. Am. Ceram. Soc.* **2015**, 98, 3236-3242.

(33) Zhu, Q.; Li, J.-G.; Zhi, C. Y.; Ma, R. Z.; Sasaki, T.; Xu, J. X.; Liu, C. H.; Li, X. D.; Sun X. D.; Sakka. Y. Nanometer-Thin Layered Hydroxide Platelets of $(Y_{0.95}Eu_{0.05})_2(OH)_5NO_3{\cdot}xH_2O$: Exfoliation-Free Synthesis, Self-Assembly, and the Derivation of Dense Oriented Oxide Films of High Transparency and Greatly Enhanced Luminescence. *J. Mater. Chem.* **2011**, 21, 6903-6908.

(34) Guo, C. F.; Luan, L.; Chen, C. H.; Huang, D. X.; Su, Q. Preparation of $Y_2O_2S:Eu^{3+}$ Phosphors by a Novel Decomposition Method. *Mater. Lett.* **2008**, 62, 600-602.

(35) Kang, C.-C.; Liu, R.-S.; Chang, J.-C.; Lee B.-J. Synthesis and Luminescent Properties of a New Yellowish-orange Afterglow Phosphor Y_2O_2S:Ti,Mg. *Chem. Mater.* **2003**, 15, 3966-3968.

(36) Ali, A. G.; Dejene, B. F.; Swart, H. C. The Influence of Oxygen Partial Pressure on Material Properties of Eu^{3+}-doped Y_2O_2S Thin Film Deposited by Pulsed Laser Deposition. *Physica B*, **2016**, 480, 174-180.

(37) Ronda, C. R.; Zeitler, G.; Schreinemacher, H.; Conrads, N.; Wiechert, D. U. Gd_2O_2S materials for use in CT application, Koninklijke Phillips Electronics, N-V-, Eindhoven (NL), United States US 2011/0114887 A1.

(38) Tan, S.; Paglieri, S. N.; Li, D. M. Nano-scale Sulfur-tolerant Lanthanide

Oxysulfide/oxysulfate Catalysts for Water-gas-shift Reaction in a Novel Reactor Configuration. *Catal. Commun.* **2016**, 73, 16-21.

(39) Zhang, D. J.; Yoshioka, F.; Ikeue, K.; Machida, M. Synthesis and Oxygen Release/Storage Properties of Ce-substituted La-oxysulfates, $(La_{1-x}Ce_x)_2O_2SO_4$. *Chem. Mater.* **2008**, 20, 6697-6703.

(40) Chen, F. S.; Chen, G.; Liu, T.; Zhang, N.; Liu, X. H.; Luo, H. M.; Li, J. H.; Chen, L. M.; Ma, R. Z.; Qiu, G. Z. Controllable Fabrication and Optical Properties of Uniform Gadolinium Oxysulfate Hollow Spheres. *Sci. Rep.* **2015**, 5, 17934.

(41) Lian, J. B.; Liu, F.; Wang, X. J.; Sun, X. D. Hydrothermal Synthesis and Photoluminescence Properties of $Gd_2O_2SO_4:Eu^{3+}$ Spherical Phosphor. *Powder Technol.* **2014**, 253, 187-192.

(42) Wang, X. J.; Li, J-.G.; Molokeev, M. S.; Wang, X. J.; Liu, W. G.; Zhu, Q.; Tanaka, H.; Suzuta, K.; Kim, B.-N.; Sakka, Y. Hydrothermal Crystallization of $Ln_2(OH)_4SO_4{\cdot}nH_2O$ Layered Compound for a Wide Range of Ln (Ln=La-Dy), Thermolysis, and Facile Transformation into Oxysulfate and Oxysulfide Phosphors. *RSC, Adv.* **2017**, 7, 13331-13339.

(43) Bruker AXS TOPAS V4: General profile and structure analysis software for powder diffraction data. - User's Manual, Bruker AXS, Karlsruhe, Germany (2008)

(44) Golovnev, N. N.; Molokeev, M. S.; Vereshchagin, S. N.; Atuchin, V. V. Synthesis and Thermal Transformation of a Neodymium(III) Complex $[Nd(HTBA)_2(C_2H_3O_2)(H_2O)_2]{\cdot}2H_2O$ to Noncentrosymmetric Oxosulfate $Nd_2O_2SO_4$. *J. Coord. Chem.* **2015**, 68, 1865-1877.

(45) Favre-Nicolin, V.; Fox, C. R. Modular Approach to Crystal Structure Determination from Powder Diffraction. *Mater. Sci. Forum.* **2004**, 443-444, 35-38.

(46) Favre-Nicolin, V.; Fox, C. R. Free Objects for Crystallography: a Modular Approach to ab Initio Structure Determination from Powder Diffraction. *J. Appl. Crystallogr.* **2002**, 35, 734-743.

(47) Xia, Z. G.; Molokeev, M. S.; Oreshonkov, A. S.; Atuchin, V. V.; Liu, R.-S.; Dong C. Crystal and Local Structure Refinement in $Ca_2Al_3O_6F$ Explored by X-ray Diffraction and Raman Spectroscopy. *Phys. Chem. Chem. Phys.* **2014**, 16, 5952-5957.

(48) Spek, A. L. Single-Crystal Structure Validation with the Program PLATON. *J. Appl. Crystallogr.* **2003**, 36, 7-13.

(49) Thompson, L. C. Complexes, in Handbook on the Physics and Chemistry of Rare Earths, ed. K. A. Gschneidner, Jr. and L. Eyring, North-Holland Physics, Amsterdam, **1979**.

(50) Rizkalla, E. N.; Choppin, G. R. Complexation Thermodynamics of Lanthanoid (III) with Ethylenediaminetetrapropionic Acid (EDTP). *J. Alloys Compd.* **1992**, 180, 325-336.

(51) Shannon, R. D. Revised Effective Ionic Radii and Systematic Studies of Interatomic Distances in Halides and Chaleogenides. *Acta Crystallogr.* **1976**, A32, 751-767.

For TOC entry only